Gas phase infrared spectroscopy of mono- and divanadium oxide cluster cations

Knut R. Asmis[a] and Gerard Meijer
Fritz-Haber-Institut der Max-Planck-Gesellschaft, Faradayweg 4-6, D-14195 Berlin, Germany

Mathias Brümmer, Cristina Kaposta, Gabriele Santambrogio, and Ludger Wöste
Institut für Experimentalphysik, Freie Universität Berlin, Arnimallee 14, D-14195 Berlin, Germany

Joachim Sauer[b]
Institut für Chemie, Humboldt-Universität Berlin, Unter den Linden 6, D-10099 Berlin, Germany

The vibrational spectroscopy of the mono- and divanadium oxide cluster cations VO_{1-3}^+ and $V_2O_{2-6}^+$ is studied in the region from 600 to 1600 wave numbers by infrared photodissociation of the corresponding cluster cation-helium atom complexes. The comparison of the experimental depletion spectra with the results of density functional calculations on bare vanadium oxide cluster cations allows for an unambiguous identification of the cluster geometry in most cases and, for VO_{1-3}^+ and $V_2O_{5,6}^+$, also of the electronic ground state. A common structural motif of all the studied divanadium cluster cations is a four-membered V–O–V–O ring, with three characteristic absorption bands in the 550–900 wave number region. For the V–O–V and V=O stretch modes the relationship between vibrational frequencies and V–O bond distances follows the Badger rule. © *2004 American Institute of Physics.* [DOI: 10.1063/1.1650833]

INTRODUCTION

Vanadium oxides are important in many technological applications,[1] e.g., in heterogeneous catalysis, semiconductors, optical devices, and coatings. The rational design of supported vanadium oxide catalysts remains difficult,[2] because of the lack of a consistent model that quantitatively explains the structure/reactivity relationship at a molecular scale. Progress is being made by applying spectroscopic methods *in situ*[3] during catalytic operation, but the identification and characterization of the active sites with currently available surface science techniques remains challenging. As many active catalysts contain vanadium oxide highly dispersed on different oxide supports, important contributions can come from gas phase cluster studies.

The formation of isolated vanadium oxide cluster cations and anions as well as their reactivity with various reactants has been studied under well-controlled conditions as a function of their size.[4–8] While mass spectrometry has become a standard technique to identify charged reactants and products and to provide information about their composition, the determination of their geometric structures remains an experimental challenge. The lack of structural knowledge together with the lack of thermochemical data so far has limited the understanding of the cluster reactivity. Attempts to predict structures from observed reactivity patterns,[6] for example, are in conflict with later predictions from reliable quantum chemical calculations. Anion photoelectron spectroscopy has proven very useful in characterizing the structure of small,

neutral vanadium oxide clusters;[5] the spectra of the larger clusters[9] are too congested to resolve any vibrational structure. The first IR spectra of individual vanadium oxide cluster cations were recently obtained from IR photodissociation studies using a tunable free electron laser.[10–12]

Quantum mechanical methods, in particular methods based on density functional theory (DFT), have proven very useful in identifying the molecular structure of metal oxide clusters in the gas phase based on a comparison of calculated and measured vibrational frequencies.[13] The electronic structure of transition metal oxides and other transition metal compounds is more difficult to calculate than main group compounds because partially filled *d* shells and the weak coupling of *d* electrons on different transition metal atoms lead to many nearly degenerate electronic states. Tests have shown[14,15] that structures of the same quality as for main group compounds can be obtained for transition metal compounds if the B3LYP hybrid density functional[16] is used. DFT predictions for structures of vanadium oxide clusters of increasing size have first been made for neutral clusters and cluster anions.[17,18] Shortly after this, predictions have also been made for the corresponding cations.[19–22] Later, the methodology first used for cluster anions[17] has been applied to cationic clusters and their reaction products with ethylene.[7,11] Reliable structure prediction is also complicated by the large number of low energy isomers in combination with many low lying electronic states. Several previous computational studies on small vanadium oxide cluster cations, for example, do not agree on the lowest electronic state and the global minimum structure, even though they apply very similar computational techniques.[7,19–21]

We recently reported a novel method[12] of measuring IR spectra of cluster ions by photodissociation of cluster ion–

---

[a]Author to whom correspondence should be addressed; electronic mail: asmis@fhi-berlin.mpg.de

[b]Author to whom correspondence should be addressed; electronic mail: sek.qc@chemie.hu-berlin.de

rare gas complexes formed in a cold ion trap. In contrast to photodissociation of the bare cluster ion predissociation of the ''messenger atom'' complex bears several important advantages. For example, the number of adsorbed photons needed to fragment the complex is considerably smaller (and often equal to one) and, more importantly, independent of the dissociation energy of the bare cluster ion. This ensures that structural isomers can be detected with the same efficiency. The present study combines this technique with a systematic DFT study in order to determine the structure of mono- and divanadium oxide cluster cations. The IR depletion spectra are compared to the DFT predictions for different low lying isomers and/or electronic states, leading to an identification of the ground state even if a global optimization method is not used.

EXPERIMENT

The present experiments were carried out on a previously described tandem mass spectrometer-ion trap system.[10] Briefly, vanadium oxide clusters are prepared by a pulsed laser vaporization source. The output of a Nd:YAG laser (Quantel Brilliant Ultra), operated at 20 Hz, is focused on a rotating 6-mm-diam vanadium rod (Alfa Aesar, 99.5% purity). The vanadium atom containing plasma is entrained in a pulse of 0.5% O_2 seeded in He carrier gas, expanded through a clustering channel and passed through a skimmer. The beam of positive ions is collimated in a radio frequency (rf) decapole ion guide and then guided into the first rf quadrupole mass filter, which is typically operated at unit resolution. Mass-selected cluster ions are guided into a cooled, He-filled ($\sim$0.02 mbar) rf hexadecapole ion trap, where they are accumulated and thermalized to the ambient temperature ($\sim$20 K) through collisions with the He buffer gas (Linde, He 6.0). Under these conditions the formation of cluster ion–rare gas atom complexes by three-body association is observed.

$$V_xO_y^+ \cdot He_{n-1} + 2He \overset{k_3}{\rightleftarrows} V_xO_y^+ \cdot He_n + He, \quad n = 1,2,...$$

as was previously reported[12] for the monovanadium oxide cluster cations. The ion concentrations are determined by the rates of the forward and the backward reaction, which depend on temperature and pressure of the He buffer gas.

IR photodissociation spectra are obtained by photoexcitation of the trapped ions with pulsed radiation from the ''free electron laser for infrared eXperiments'' (FELIX),[23] which is operated at 5 Hz. A measurement cycle is initiated by the trigger signal of the previous FELIX pulse and the ion trap is allowed to fill with mass-selected ions for a fixed time t_{fill}. Next, the ions are allowed to thermalize, which is assumed to proceed on a time scale of up to a few milliseconds. Then, the accumulated, cooled ions are irradiated inside the ion trap. Directly after FELIX fires, all ions are extracted and the mass-selected ion yield is monitored. This cycle is repeated multiple times (3–10 times for the present experiments) and then FELIX is set to the next wavelength. Resonant absorption of IR radiation by the ion complexes leads to vibrational predissociation of the complexes. Consequently, the ion concentration of the (absorbing) complex

decreases and that of the bare ion increases temporarily, until the system is able to dissipate all the absorbed energy and return to equilibrium. Thus, if the rate of reformation is slow enough, the infrared spectroscopy of the parent ions $V_xO_y^+$ can be studied by mass-selectively monitoring changes in the $V_xO_y^+ \cdot He_n$ ion yield as a function of photon wavelength directly after irradiation with a tunable IR source.[12] The dependence of the dissociation rate on the initially excited vibrational mode is assumed to be negligible, because, under the present experimental conditions, there is sufficient time (microseconds or more) for the efficient redistribution of the excitation energy. Ideally, with t_{fill} less than 200 ms, the experiment can make use of the FELIX repetition rate of 5 Hz. In practice, longer filling times proved to yield superior signal statistics. An acquisition time $t_{fill} = 600$ ms was used throughout the experiments described here.

In the present study overview spectra are measured in the region from 6 to 16 μm with a step size of 0.1 μm. Spectra with smaller step sizes and longer accumulation times are then measured in those spectral regions, where signal was observed. The output of FELIX is introduced into the ion trap region through a ZnSe window, a 50 cm focal length KBr lens, and a 5-mm-thick KBr window. Focusing of the FELIX beam is required to avoid light scattering off the ion trap exit and entrance lenses. The transmission of the KBr optics is nearly wavelength independent in the region studied. The transmission of the ZnSe window decreases considerably at longer wavelengths. The accuracy of the determined vibrational frequencies is generally within 1% of the central wavelength. The accuracy of the relative depletion intensities is less well defined, mainly due to the non-monotonic variation of the FELIX beam intensity, bandwidth, and waist size with wavelength. We did not correct for any of these effects and estimate that our relative intensities vary within 10% between 1200 and 700 cm^{-1} and to a larger extent in the region below 700 cm^{-1}.

COMPUTATIONAL METHODS

All calculations are carried out using the TURBOMOLE suite of programs.[24] The B3LYP hybrid functional[16] employed combines Becke's 1988 nonlocal exchange[25] with Hartree–Fock exchange along with the Lee–Yang–Parr[26] correlation functional. Note that other implementations[27] of the B3LYP functional use a slightly different formulation of the Vosko-Wilk-Nusair (VWN) local correlation functional.[28] The TZVP basis sets applied are the triple-zeta valence basis sets developed by Ahlrichs and co-workers[29] augmented by polarization functions, a d set for oxygen and a p set for vanadium.[30] Harmonic vibrational frequencies are obtained from second analytic derivatives.[31] Structure optimizations use tight convergence criteria. Structures are optimized until Cartesian gradients are smaller than 1×10^{-4} Hartree/Bohr and the energy change smaller than 1×10^{-6} Hartree. The self-consistent field convergence criterion is 1×10^{-7} Hartree for the energy and 1×10^{-7} a.u. for the root-mean square of the density.

It is known that B3LYP vibrational frequencies are systematically too large (see, e.g., Refs. 32 and 33) and, therefore, agreement with observed frequencies can be improved

TABLE I. Frequency scaling factors for fundamental vibrations and root-mean-square deviation (rms) derived from a least squares fit of frequencies.

	No. of data	Scale factor	rms (cm^{-1})
(1a) Vanadyl modes only[a]	10	0.9167	13
(1b) V–O–V modes only[a]	14	0.9832	26
(2) All modes[a]	24	0.9429	35
Ref. 32	1066	0.9614	34
Ref. 33	900	0.9726	42

[a]Present study.

by scaling. Scaling accounts for both anharmonicities (calculated harmonic wave numbers are compared to observed fundamentals including anharmonicities) and systematic errors of the calculated harmonic force constants. For the systems studied anharmonicity effects are expected to be small. We use 24 experimental vibrational frequencies of VO^+(1), VO_2^+(2), $V_2O_2^+$(2), $V_2O_3^+$(4), $V_2O_4^+$(5), $V_2O_5^+$(5), and $V_2O_6^+$(5). The two unassigned modes in VO_3^+ and the superoxo mode in $V_2O_6^+$ are not used. Following the procedure described by Scott and Radom,[32] two different types of scaling are done: (1) Individual scaling for two groups of frequencies, (a) vanadyl stretch vibrations (10 values) and (b) V–O–V stretch and all other vibrations below 900 cm^{-1} (14 values). (2) Global scaling using all 24 frequencies. Table I shows the results. The scale factors obtained and the root-mean-square deviations of the scaled frequencies fall into the known ranges.[32,33]

RESULTS

Optimized B3LYP/TZVP geometries of selected mono- and divanadium oxide cluster cations are shown in Fig. 1 and their vibrational frequencies are listed in Table II. Infrared photodissociation spectra of the vanadium oxide cluster cations VO_{1-3}^+ and $V_2O_{2-6}^+$, measured by monitoring the depletion of the respective cluster ion–He_n complex ($n=1$, 2, or 3), are shown in Figs. 2–4. Experimental vibrational frequencies (band centers) are listed in Table II. $He_{n>1}$ complexes were monitored, whenever the depletion signal of the He_1 complex was weak or completely masked either due to partial dissociation of $He_{n>1}$ complexes or rapid reformation dynamics. In all cases the influence of the He atoms on the vibrational frequency is assumed to be small, i.e., on the order of a few wave numbers or less. Rotationally resolved vibrational predissociation experiments on proton-bound He complexes revealed redshifts up to 15 cm^{-1} for hydrogen stretching motions, corresponding to less than 0.5% of the fundamental frequency.[34] Due to the considerably higher reduced mass and lower vibrational frequency of the modes considered here, the frequency shift should be comparably smaller. For $V_2O_2^+$ the signal level was very low and the spectra of two different complexes ($n=2$ and $n=3$) were summed. The simulated spectra are based on globally scaled harmonic frequencies and relative intensities determined by B3LYP/TZVP calculations, and were convoluted with a Gaussian line shape function, with a width that increases linearly with increasing frequency, in order to correct for the wavelength dependent bandwidth of FELIX. The experimen-

tal data are plotted against a logarithmic scale to aid in the comparison to the simulated absorption spectra. According to Lambert–Beer's law, the logarithm of the relative depletion (I/I_0) is proportional to the absorption coefficient. Furthermore, it is assumed that if a photon is absorbed, it always leads to dissociation with probability that is independent of wavelength. Binding energies of He atoms to ionic complexes[35] are on the order of a few hundred wave numbers or less and thus a single IR photon should be sufficient to dissociate the ion-He atom complexes studied here.

VO^+

The IR depletion spectrum of $VO^+ \cdot He$ (Fig. 2, left) reveals a single band at 1053 cm^{-1}. Upon closer inspection the band shows additional structure, a double minimum feature, which is attributed to the influence of molecular rotations discussed elsewhere in more detail.[12] The center of the band remains nearly unchanged in the spectra of the $VO^+ \cdot He_2$ (1053 cm^{-1}) and $VO^+ \cdot He_3$ (1054 cm^{-1}) complexes (not shown), confirming that the He atoms have a negligible influence on the V–O stretching frequencies. The position of the band center is in good agreement with, but significantly more accurate than, the value obtained for the $^3\Sigma^-$ ground state of bare VO^+ using photoelectron spectroscopy (1060 ± 40 cm^{-1}).[36] The recent high-level *ab initio* calculations (multi-reference average coupled pair functional, MR-ACPF, with basis set extrapolation) of Pykavy and van Wüllen[37] for bare VO^+ yield 1058 cm^{-1}. Our B3LYP/TZVP frequency ($\nu_{scaled}=1032$ cm^{-1}) is in reasonable agreement with these results, as is the calculated bond length ($r_e=1.55$ Å), which was determined experimentally ($r_0=1.56$ Å) from rotationally resolved pulsed field ionization spectra.[38]

VO_2^+

Two bands are observed in the depletion spectrum of $VO_2^+ \cdot He_2$ (Fig. 2, right) at 1017 and 990 cm^{-1} with relative intensities of 1–3. Both, the intensity ratio and the splitting of the two bands, are reproduced well by the B3LYP/TZVP calculations, confirming the bent $^1A_1$ ground state for VO_2^+, originally proposed by Harvey *et al.*[8] The two bands are assigned to the symmetric ($\nu_{scaled}=1038$ cm^{-1}) and antisymmetric ($\nu_{scaled}=1011$ cm^{-1}) stretch mode, respectively. The energy of the bending mode, predicted at $\nu_{scaled}=445$ cm^{-1} with a relative intensity of 3%, is too small to be observed in the present spectra. The spectrum[20] of the lowest triplet state, an $^3A''$ state 156 kJ/mol above the $^1A_1$ ground state, with vibrational frequencies of 1171 and 690 cm^{-1}, clearly does not match the experimental spectrum.

VO_3^+

The depletion spectrum of $VO_3^+ \cdot He_2$ (Fig. 3, left) shows two bands. The most intense feature is found at 1069 cm^{-1}. The second peak lies 32 cm^{-1} lower in energy and is roughly half as intense. Overview scans down to 625 cm^{-1} (not shown) revealed no additional signal at lower photon energies. The lowest electronic state predicted by our B3LYP calculations is the open-shell $^3A''$ state with an oxovanadium(V)-η^2-superoxide structure, also found in the
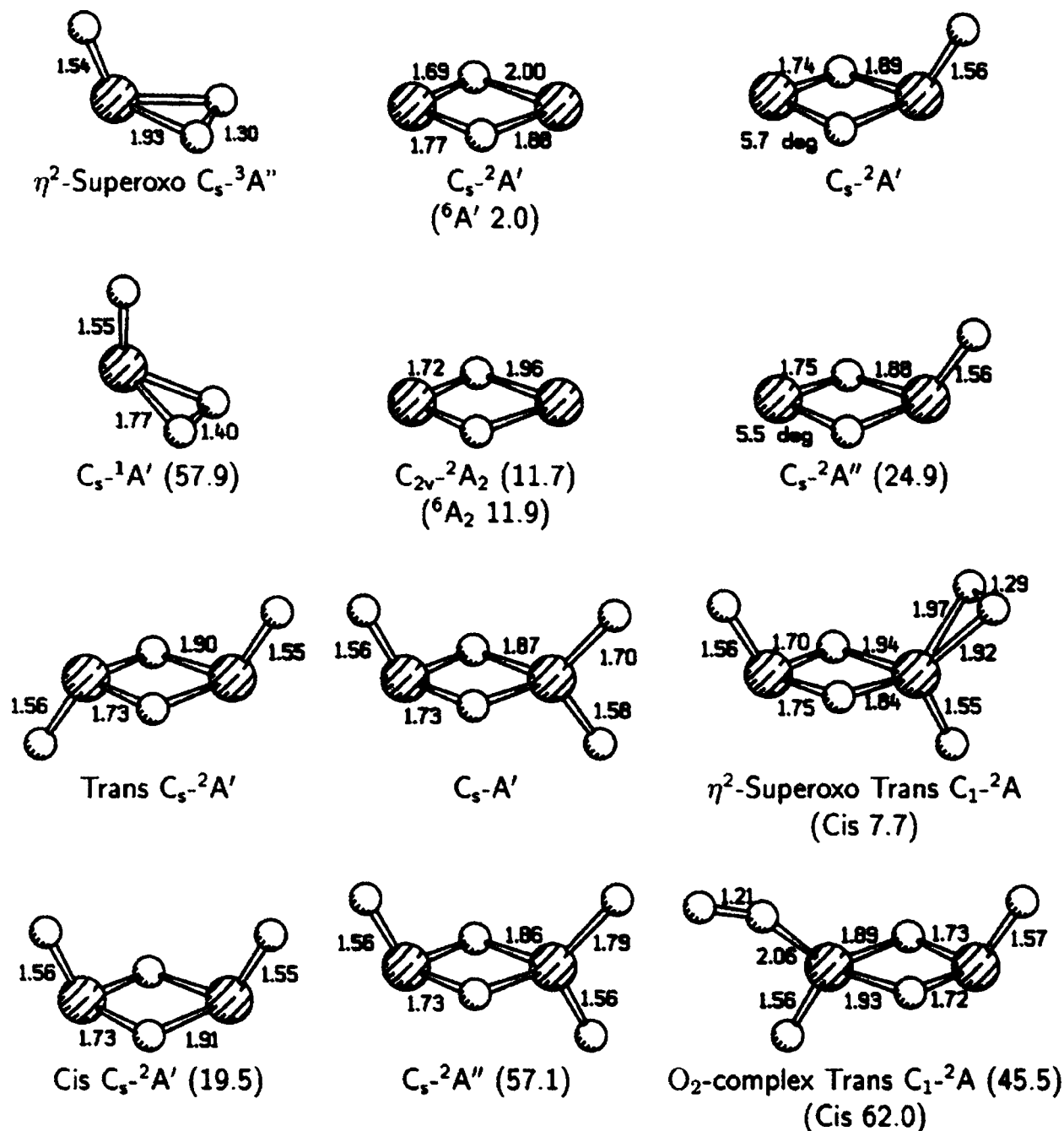
FIG. 1. B3LYP/TZVP optimized structures of selected mono- and divanadium oxide cluster cations. Two structures are shown for each cluster, one of the electronic ground state (top) and the other of an energetically low-lying isomer (bottom). Bond lengths are in Å, bond angles in degrees, and relative energies (in parentheses) with respect to the ground state are in kJ/mol. The structures of VO^+ and VO_2^+ are shown in Fig. 2.

previous calculations by Koyanagi *et al.*[19] Another study[20] proposed an $^1A'$ ground state, but did not consider the $^3A''$ state of the η^2-superoxo structure. We find this $^1A'$ state 57.9 kJ/mol above the $^3A''$ ground state. Both states have similar geometries (see Fig. 1), but characteristically different IR spectra (see Fig. 3). The dioxo group in the $^1A'$ state has larger O–O and smaller OV–O_2 bond lengths, but a stronger redshift of the O–O stretch, 1051 cm^{-1} compared to 1126 cm^{-1} in the $^3A''$ state. Moreover, the spectrum of the $^1A'$ state shows several peaks at low photon energies. Summarizing, we find significantly better agreement between the experimental and calculated spectra of the ground electronic

state ($^3A''$) than for the lowest singlet state ($^1A'$). The assignment of the individual bands, one to the vanadyl- and the other to the oxo-mode, is left open, because the predicted intensity ordering does not match the experimental spectrum.

$V_2O_2^+$

In contrast to the spectra of the monovanadium oxide cluster cations discussed above, the depletion spectra of $V_2O_2^+ \cdot He_{2,3}$ (Fig. 3, center) do not show any features above 900 cm^{-1}, but rather two bands of similar intensity are found at lower photon energies, namely at 833 and 724 cm^{-1}.

J. Chem. Phys., Vol. 120, No. 14, 8 April 2004

Spectroscopy of vandium oxide cluster cations   6465

TABLE II. Experimental (v_{expt}), calculated (v_{B3LYP}), and scaled (v_{scaled}) vibrational frequencies, relative intensities (in parentheses), and frequency difference $\Delta v = v_{scaled} - v_{expt}$ for mono- and divanadium oxide cluster cations. All frequencies are in wave numbers. Experimental frequencies are based on the IR depletion spectra of the corresponding $V_xO_y^+ \cdot He_n$ cluster ions. Theoretical values are determined by B3LYP/TZVP calculations. Scaled frequencies are calculated using the individual scaling factors (1a,b in Table I).

Experiment		B3LYP calculations					
System	v_{expt}	State	v_{B3LYP}	Sym.	Type	v_{scaled}	Δv
$VO^+ \cdot He$	1053	$^3\Sigma^-$	1125 *(1.00)*	a_1	Vanadyl	1032	−21
$VO_2^+ \cdot He_2$	1017	$^1A_1$	1133 *(0.13)*	a_1	Vanadyl	1038	+21
	990		1103 *(1.00)*	b_1	Vanadyl	1011	+21
$VO_3^+ \cdot He_2$	1069[a]	$^3A''$	1228 *(0.52)*	a'	Oxo	1126[b]	
	1037[a]		1161 *(1.00)*	a'	Vanadyl	1064	
$V_2O_2^+ \cdot He_{2,3}$	833	$^2A'$	849 *(1.00)*	a'	Ring	835	+2
	724		712 *(0.98)*	a'	Ring	700	−24
			575 *(1.32)*	a'	Ring	565	
$V_2O_3^+ \cdot He_3$	1044	$^2A'$	1127 *(0.63)*	a'	Vanadyl	1033	−11
	803		823 *(0.46)*	a'	Ring	809	+6
	765		718 *(0.62)*	a''	Ring	706	−59
	666		638 *(1.00)*	a'	Ring	627	−39
$V_2O_4^+ \cdot He_3$	1049	$^2A'$	1135 *(0.19)*	a'	Vanadyl	1041	−8
	1029		1116 *(1.00)*	a'	Vanadyl	1023	−6
	794		844 *(0.43)*	a'	Ring	830	+36
	776		774 *(0.47)*	a''	Ring	761	−15
	594		637 *(0.75)*	a'	Ring	627	+33
$V_2O_5^+ \cdot He$	1034	$^2A'$	1130 *(0.52)*	a'	Vanadyl	1036	+2
	911		1005 *(0.54)*	a'	Vanadyl	921	+10
	815		850 *(0.66)*	a'	Ring	835	20
	738		749 *(0.46)*	a''	Ring	736	−2
	657		679 *(1.00)*	a'	Ring	668	11
			597 *(0.00)*	a'	V–O	587	
$V_2O_6^+ \cdot He$	1160	$^2A'$	1246 *(0.31)*	a	Oxo	1142[b]	−18
	1060		1149 *(0.34)*	a	Vanadyl	1054	−6
	1028		1121 *(0.80)*	a	Vanadyl	1028	0
	836		873 *(0.66)*	a	Ring	859	23
	751		765 *(0.37)*	a	Ring	752	+1
	673		677 *(1.00)*	a	Ring	665	−8

[a]Not assigned.
[b]Scaled with vanadyl scaling factor.

Therefore the presence of vanadyl (or oxo) groups, which would be expected in the region above 900 cm^{-1}, can be excluded. The width of the observed bands is somewhat larger than for the other systems studied. This is a result of the low parent ion signal level, which we compensated by increasing the FELIX power and thus also its bandwidth. Satisfactory agreement is found with the simulated IR spectra of the lowest energy isomer, an $^2A'$ state with a planar, four-membered V–O–V–O ring. Of the six vibrational modes, the three highest in energy ($v_{scaled} = 835$, 700, and 565 cm^{-1}) are predicted to be the most intense and therefore they comprise the spectroscopic "fingerprint" of the ring structure. All three of these modes are in-plane deformation modes. The two higher modes match well with the experimental spectrum, while the lowest one lies too low in energy to be observed in our spectra. Note, for the larger cluster ions, starting with $V_2O_3^+$, this third band is blueshifted and consequently all three modes comprising the fingerprint are observed in the spectra of the larger species.

A cyclic $^2A'$ ground state agrees with the previous study of Calatayud *et al.*[20] However, the next electronic state is not $^4B_2$ but $^6A'$. Due to the weak coupling of *d* electrons on the two vanadium sites the $^6A'$ high-spin analogue of $^2A'$ is
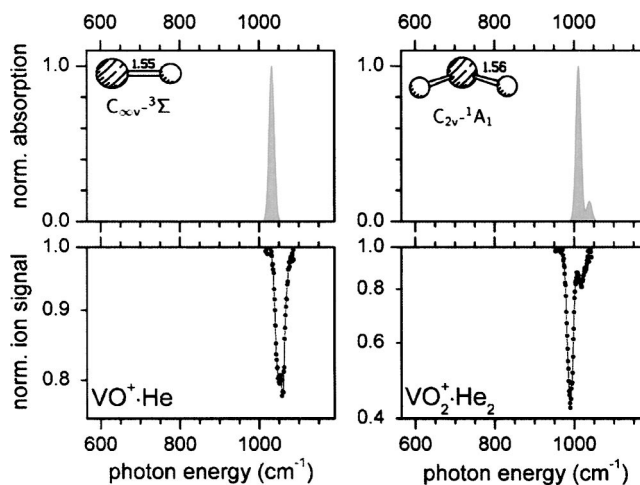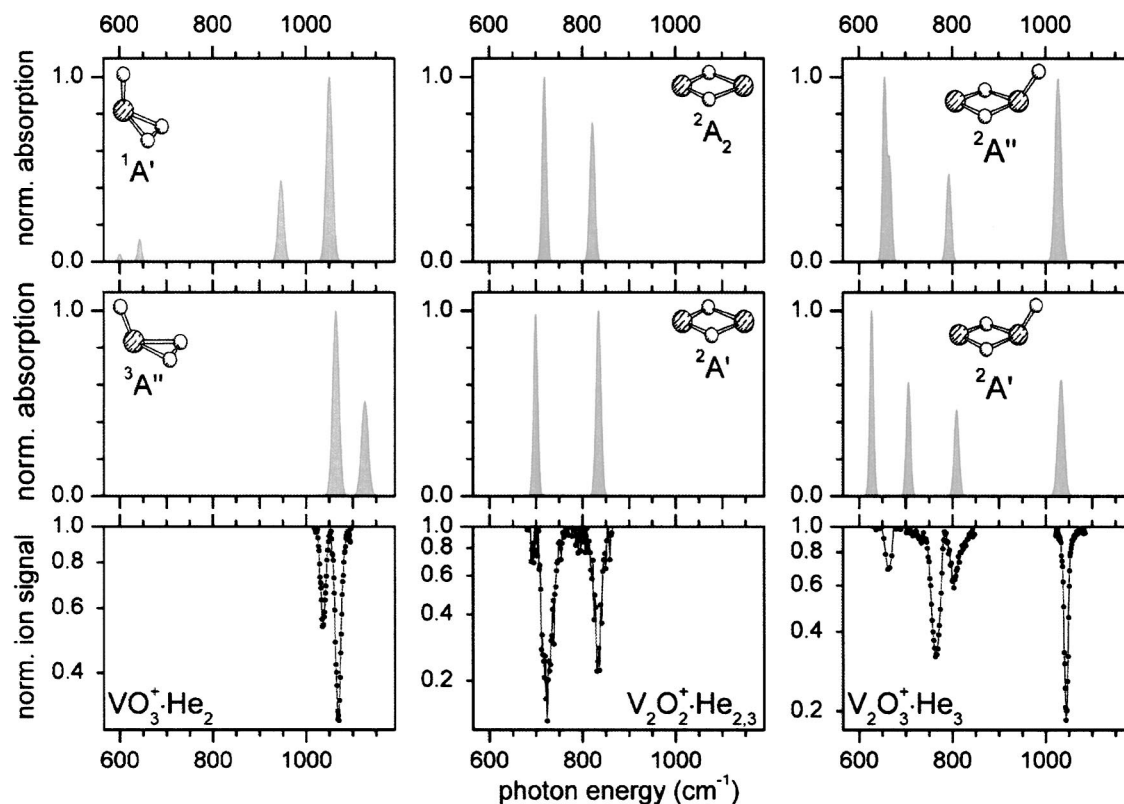

FIG. 2. Simulated IR absorption spectrum (gray line and gray shaded area), based on scaled B3LYP/TZVP frequencies and relative intensities of the ground state (top row) of VO^+ (left) and VO_2^+ (right) in the region from 565 to 1190 cm^{-1}. Higher resolution, experimental IR photodepletion spectrum (solid black dots connected by black lines) of $VO^+ \cdot He$ (left) and $VO_2^+ \cdot He_2$ (right) in this energy region are shown in the bottom row. Note the logarithmic scale for the ion signal.

FIG. 3. Simulated IR absorption spectra (gray line and gray shaded area), based on scaled B3LYP/TZVP frequencies and relative intensities of the ground state (middle row) and lowest, electronically excited state (top row), of VO_3^+ (left), $V_2O_2^+$ (middle), and $V_2O_3^+$ (right) in the region from 565 to 1190 cm^{-1}. Higher resolution, experimental IR photodepletion spectrum (solid black dots connected by black lines) of $VO_3^+ \cdot He_2$ (left), $V_2O_2^+ \cdot He_{2,3}$ (center), and $V_2O_3^+ \cdot He_3$ (right) in this energy region are shown in the bottom row. Note the logarithmic scale for the ion signal.

only two kJ/mol higher in energy and has a virtually identical IR spectrum. A $^2A_2$ state (C_{2v} symmetry), with a very similar IR spectrum (see Fig. 3) and slightly better agreement with the experimental spectrum, is found only 10 kJ/mol above the $^2A'$ state. Its high-spin analog, an $^6A_2$ state, is only 0.2 kJ/mol above the $^2A_2$ state. Therefore an unambiguous assignment of the electronic ground state of $V_2O_2^+$ requires higher level calculations.

$V_2O_3^+$

The depletion spectrum of $V_2O_3^+ \cdot He_3$ is shown on the right of Fig. 3. A single, intense band (1044 cm^{-1}) lies in the vanadyl-stretch region. Three additional bands are observed below 810 cm^{-1}, in the V–O–V–O ring fingerprint region. Consequently, the spectrum supports a ring structure with a single, exocyclic vanadyl group, in contrast to, for example, a linear chain structure, which would reveal two characteristic vanadyl bands.[20] The experimental spectrum is in reasonable agreement with the IR spectrum of the lowest electronic state ($^2A'$) found in our and previous[20] calculations. In particular, the number and position of the IR active bands are reproduced satisfactorily. The largest discrepancy is observed for the relative intensity of the 666 cm^{-1} band. The lowest excited state is an $^2A''$ state, which lies 24.9 kJ/mol above the $^2A'$ state. Its absorption spectrum reveals only three bands plus a shoulder and agrees less well with the observed one.

$V_2O_4^+$

The IR photodissociation spectrum of $V_2O_4 \cdot He_3$ shows four bands at 1049, 1029, 776, and 594 cm^{-1} and a pronounced shoulder at 794 cm^{-1} (see Fig. 4, left). In line with the arguments given above and our calculations for $V_2O_4^+$, the three features below 800 cm^{-1}, of which the higher two partially overlap, are attributed to the characteristic modes of the V–O–V–O ring subunit and the two peaks above 1000 cm^{-1} are assigned to the symmetric (1049 cm^{-1}) and the antisymmetric (1029 cm^{-1}) combination of the two exocyclic vanadyl groups, with the antisymmetric stretch being the more intense of the two bands. The two vanadyl groups may either occupy cis or trans positions with respect to the ring plane. Note, that a comparison of the relative intensities of all bands would favor an assignment to the cis isomer. However, our B3LYP/TZVP calculations place the cis isomer 19.5 kJ/mol higher in energy than the trans isomer. This gap is reduced to 8.4 kJ/mol, when high-level *ab initio* calculations (MR-ACPF with basis set extrapolation at the B3LYP geometry) are performed.[15] Since in $V_2O_4^+$ the unpaired *d* electron localizes at one of the V sites, the V–O–V–O ring has two long and two short V–O bonds. Isomerization into the equivalent structure with the *d* electron at the other V site is possible for both the trans and cis structure via a symmetric transition structure (C_{2h} and C_{2v} symmetry, respectively) with four identical V–O bonds in the ring.[15] The energy barriers are 19.4 and 21.2 kJ/mol, respectively.[15] At suffi-
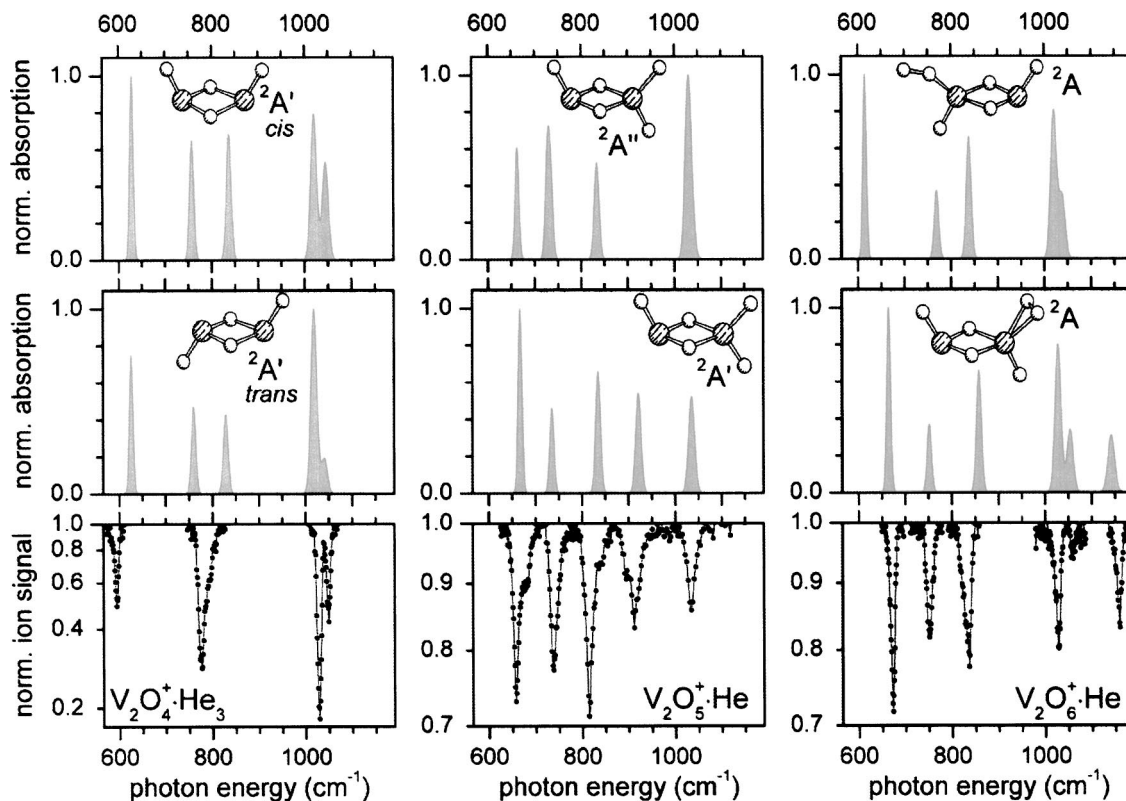
FIG. 4. Simulated IR absorption spectra (gray line and gray shaded area), based on scaled B3LYP/TZVP frequencies and relative intensities of the ground state (middle row) and an energetically low-lying isomer (top row), of $V_2O_4^+$ (left), $V_2O_5^+$ (middle), and $V_2O_6^+$ (right) in the region from 565 to 1190 cm^{-1}. Higher resolution, experimental IR photodepletion spectrum (solid black dots connected by black lines) of $V_2O_4^+ \cdot He_3$ (left), $V_2O_5^+ \cdot He$ (center), and $V_2O_6^+ \cdot He$ (right) in this energy region are shown in the bottom row. Note the logarithmic scale for the ion signal.

ciently high temperatures large amplitude motions along this isomerization coordinate may affect the predictions for the highest (830 cm^{-1}) and lowest (627 cm^{-1}) of the three characteristic V–O–V–O ring modes which are due to stretches of the V–O bonds in the ring (see Fig. 5).
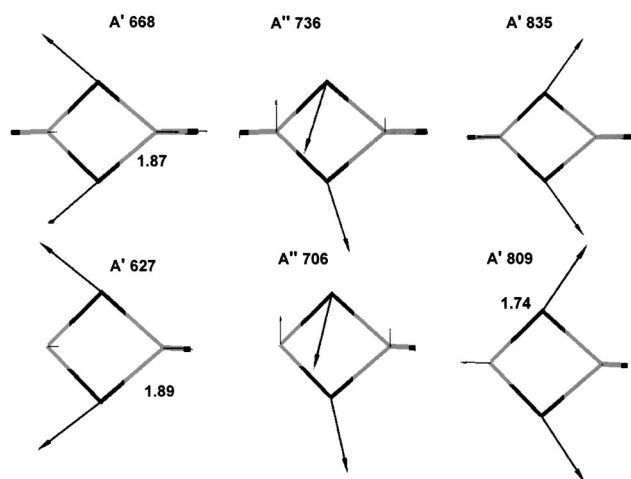

FIG. 5. The three characteristic "in-plane" normal modes of the central V–O–V–O ring in divanadium oxide cluster cations. The relative motion of the atoms, which is predominantly limited to motion in the plane of the ring, is indicated by the arrows. The scaled B3LYP/TZVP vibrational frequencies are (from left to right) 668, 736, and 835 cm^{-1} for $V_2O_5^+$ (top row) and 627, 706, and 809 cm^{-1} for $V_2O_3^+$ (bottom row).

$V_2O_5^+$

The IR photodissociation spectrum of $V_2O_5^+ \cdot He$ (Fig. 4, bottom row, center) shows five bands, two bands in the vanadyl region at 1034 and 911 cm^{-1} and three, roughly twice as intense bands, below 900 cm^{-1} at 815, 738, and 657 cm^{-1}. In addition, shoulders are observed at 896, 839, and 679 cm^{-1}. The position, as well as the intensity pattern of the five main peaks, is in excellent agreement with the simulated IR spectrum of the $^2A'$ state (see Fig. 4), the lowest electronic state we find in our B3LYP/TZVP calculations. Based on these calculations, the 1034 cm^{-1} band, calculated at $\nu_{scaled} = 1036$ cm^{-1}, is assigned to the stretch mode of the isolated vanadyl bond (see Fig. 1). The two geminal V–O bonds form a symmetric and an antisymmetric combination delocalized over both bonds, with scaled frequencies of 922 and 587 cm^{-1}, respectively. The antisymmetric combination is assigned to the 911 cm^{-1} feature in the experimental spectrum, while the 587 cm^{-1} band has virtually no intensity (although IR allowed) and is not observed. Similar to the assignments for $V_2O_{2-4}^+$, the remaining three intense bands below 900 cm^{-1} are attributed to the three characteristic modes of the central V–O–V–O ring.

The next highest electronic state, calculated 57.1 kJ/mol above the ground state, has $^2A''$ symmetry and geometrical parameters which are similar to those of the $^2A'$ ground state. The main difference between the two structures is in the length of the longer of the two geminal V–O bonds (cis

position to the isolated V–O bond). In the $^2A'$ state the bond distances for the geminal V–O bonds are 170 and 158 pm, while in the $^2A''$ state they are 179 and 156 pm. The effect on the IR spectrum is substantial. In contrast to the $^2A'$ state, the two geminal V–O bond stretches do not mix, but remain predominantly localized on the longer and shorter V–O bond, and both have appreciable intensity. The scaled frequency of the mode involving the shorter bond is 1030 cm^{-1}, minimally lower than the frequency of the mode involving the isolated vanadyl bond (1038 cm^{-1}). Consequently, the two modes lead to overlapping bands and form a single, intense feature in the simulated spectrum. The scaled frequency of the mode involving the longer V–O bond is 728 cm^{-1} and overlaps with one of the three ring breathing modes (834, 736, and 663 cm^{-1}), effectively increasing the relative intensity of the central feature of this group of three bands. The predicted spectrum of the $^2A''$ state cannot explain the band observed at 911 cm^{-1} and we conclude that the calculated B3LYP/TZVP energies and the comparison of the IR spectra provide convincing evidence for an $^2A'$ and against an $^2A''$ ground state of V$_2$O$_5^+$. The origin of the observed shoulders is not clear and they are left unassigned. Note, the position of the shoulders does not match the absorption spectrum of the $^2A''$ excited state discussed above.

V$_2$O$_6^+$

The IR photodissociation spectrum of V$_2$O$_6^+$·He is shown on the right of Fig. 4. Six bands are observed. The band at 1160 cm^{-1} is too high in energy for a regular vanadyl group and thus is assigned to a superoxo group. The two bands at 1060 and 1028 cm^{-1} lie in the typical spectral region for vanadyl stretches. Similar to the other spectra of divanadium oxide cluster cations, the three bands at 836, 751, and 673 cm^{-1} are attributed to the three characteristic modes of a four-membered V–O–V–O ring. The experimental spectrum matches exceptionally well with the spectrum calculated for the ^2A ground state of V$_2$O$_6^+$, and clearly disagrees with the spectrum of the "O$_2$-complex" isomer (^2A), found 45.5 kJ/mol above the ground state. In the ground state of V$_2$O$_6^+$ the two vanadyl groups occupy the trans position and the η^2-superoxo unit forms a three-membered ring with one of the two vanadium atoms (see Fig. 1). The cis isomer is calculated 7.7 kJ/mol higher in energy. Its IR spectrum is virtually identical with that of the trans isomer and not shown.

DISCUSSION

Comparison of the present results with previous multiphoton IR photodissociation studies on metal oxide cations in the region below 2000 cm^{-1} highlights several important features of the current experimental scheme. (1) In most previous studies on cluster ions and using free electron laser (FEL) radiation the initial ion beam was not mass selected (see, for example, Ref. 39 and references therein) and consequently a mass distribution of cluster ions is irradiated. A mass filter is then used to mass select the "product" ions. Although this method has the multiplex advantage, this procedure does not uniquely identify the signal carrier, because

product ions of identical mass can be formed from different parent ions. Unless one has a detailed understanding of the dissociation pathways, mass selection of the ions *prior* to irradiation is required in order to unambiguously identify the signal carrier. (2) IR photodissociation experiments on bare metal oxide clusters generally require the absorption of multiple IR photons. When multiple isomers are present in the ion beam, the isomer with the lowest dissociation energy, which does not necessarily have to be the thermodynamically most stable one, generally dissociates at the lowest laser fluence and thus is most facile to detect. IR multiphoton dissociation studies on V$_4$O$_{10}^+$, for example, showed that a V$_4$O$_8^+$·O$_2$ isomer could be detected, but not the theoretically predicted most stable cage-like isomer of V$_4$O$_{10}^+$, because the dissociation energy is more than 3 eV higher for the cage structure.[10] He tagging reduces the number of photons required in the photodissociation process dramatically, generally down to a single photon, avoiding the complications described above. (3) He tagging also results in a considerable increase of the spectral resolution, because the absorbing species are necessarily the colder subset of the species present in the ion trap, and generally much colder compared to those produced directly by laser vaporization.

The improved experimental scheme combined with the reliable prediction of ground state geometries and frequencies allows for a detailed insight into the structure of metal oxide cluster ions in general and of vanadium oxide cluster cations in this particular study. The central building block of the divanadium oxide cations is a four-membered V$_2$O$_2$ ring, in which each vanadium atom is adjacent to two oxygen atoms. For one vanadium atom the two V–O bonds are significantly shorter than for the other. Experimental evidence for four-membered rings as a structural motif in metal oxide clusters was originally found by von Helden *et al.*[13] in their pioneering study on the infrared spectroscopy of neutral zirconium oxide clusters. They observed two very broad absorption bands centered at 620 and 680 cm^{-1}, respectively, and assigned them to vibrational modes of the Zr–O–Zr–O ring, predicted in the 600–800 cm^{-1} range. The spectral signature of the V–O–V–O four-membered ring is three absorption bands of comparable intensity in the region from 550 to 900 cm^{-1}. Both the observed and predicted (in parenthesis) wave numbers fall into narrow ranges of 833–794 (859–809), 776–724 (761–700), 673–594 (668–565) cm^{-1}. As the oxygen content increases from V$_2$O$_2^+$ to V$_2$O$_6^+$, the number of unpaired d electrons on vanadium sites decreases from 3/2 in V$_2$O$_2^+$ to 1/0 in V$_2$O$_6^+$ and the number of terminal VO groups increases from none to 3. V$_2$O$_6^+$ includes an additional η^2-superoxo ligand. Neither of these changes affects the characteristic V$_2$O$_2$ ring modes significantly. Figure 5 sketches the three modes. The highest and the lowest energy modes are couplings of the stretches of the two shorter and longer VO bonds, respectively, with the deformation of the opposite V–O–V angle. Their splitting is indicative of the asymmetry of the VO bond distances in the ring. The third mode is a O–V–O twist.

The present data can be used to deduce information about V–O bond distances of vanadium oxide species, for which the IR spectra (or Raman spectra) are known, but the
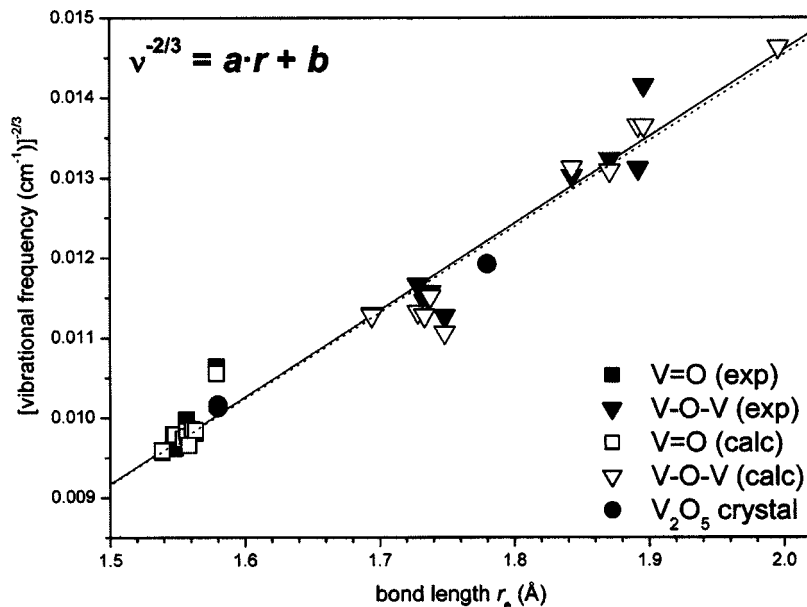
FIG. 6. Badger's rule plot of $\nu^{-2/3}$ against the r_e, where ν is the vanadium–oxygen stretching frequency and r_e the vanadium–oxygen bond length. Scaled harmonic (open symbols) and experimental (solid symbols) vibrational frequencies are shown. Squares and triangles refer to gas phase values from the present study and the solid circles are based on previous results on crystalline V_2O_5. For the gas phase, data squares indicate frequencies for terminal $V\!\!=\!\!O$ bonds, while triangles represent V–O–V bonds including divalent oxygen atoms. Solid and dotted lines represent the linear, least squares fit to the experimental (gas phase only) and calculated frequencies, respectively.

structure is not. This is relevant for supported vanadium oxide catalysts, and attempts have been made to predict vanadium oxide bond distances for solid materials of unknown structure involving vanadium oxides.[40] Figure 6 shows that the frequencies of the vanadium–oxygen stretch modes are indeed a monotonic function of the bond distance. Based on the Badger rule, which assumes that for a given bond type the harmonic force constant k is inversely proportional to the cube of the bond distance r_e, $k = C/(r_e - d)^3$, $\nu^{-2/3}$ is plotted against the equilibrium bond distance r_e. Both scaled harmonic (open symbols) and experimental (solid symbols) vibrational frequencies are shown. Squares indicate terminal $V\!\!=\!\!O$ bonds, while triangles represent V–O–V bonds including divalent oxygen atoms. Solid and dotted lines represent the linear, least squares fit to the experimental and theoretical frequencies, respectively. The linear fit yields similar values for the experimental ($a = 0.010\,86$ cm$^{2/3}$/Å, $b = 0.007\,13$ cm$^{2/3}$) and the theoretical frequencies ($a = 0.010\,76$ cm$^{2/3}$/Å, $b = 0.006\,98$ cm$^{2/3}$). Included in the figure are also observed data for $V\!\!=\!\!O$ and V–$O(-V)$ bonds of crystalline V_2O_5 (solid circles). The observed IR frequencies (981/976 and 768 cm^{-1}, respectively)[41] and bond distances (1.58 and 1.78 Å, respectively) derived from the x-ray structure[42] fall on the same line. Hence, use may be made of the present data to derive structure information from IR or Raman spectra of vanadium oxide species supported, for example, on aluminum oxide and silicon dioxide.

Previous theoretical studies had predicted the correct connectivity for most of the clusters, however conflicting assignments for the electronic ground states of VO_3^+, $V_2O_2^+$, $V_2O_4^+$, $V_2O_5^+$, and $V_2O_6^+$ were made. The assumption of a $^2A''$ ground state in $V_2O_5^+$ in Ref. 7 is of particular significance, as many of the reaction energies and also the energy profile shown in Fig. 4 of Ref. 7 will change if the $^2A'$ ground state found in the present and a previous study[21,43] is considered. Our calculation of the reaction energies in Table I of Ref. 7 shows that all four reaction energies for $V_2O_5^+ + C_2H_4$ and two of the reaction energies for $V_2O_6^+ + C_2H_4$ change by about 0.6 eV. Since the changes for $V_2O_5^+$ and $V_2O_6^+$ are in opposite direction, the predicted reactivity differences between the two oxide species become significantly smaller and additional effort is needed to fully understand the observed reaction patterns.

ACKNOWLEDGMENTS

[1] C. N. R. Rao and B. Raven, *Transition Metal Oxides* (VCH, New York, 1995).

[2] B. M. Weckhuysen and D. E. Keller, Catal. Today **78**, 25 (2003).

[3] G. G. Cortez and M. A. Banares, J. Catal. **209**, 197 (2002).

[4] D. Schröder, J. Loos, M. Engeser, H. Schwarz, H.-C. Jankowiak, R. Berger, R. Thissen, O. Dutuit, J. Döbler, and J. Sauer, Inorg. Chem. (in press); E. B. Rudnyi, E. A. Kaibicheva, and L. N. Sidorov, J. Chem. Thermodyn. **25**, 929 (1993); R. C. Bell, K. A. Zemski, and A. W. Castleman, Jr., J. Phys. Chem. A **102**, 8293 (1998); R. C. Bell, K. A. Zemski, and A. W. Castleman, Jr., *ibid.* **103**, 1585 (1999); R. C. Bell, K. A. Zemski, D. R. Justes, and A. W. Castleman, Jr., J. Chem. Phys. **114**, 798 (2001); K. A. Zemski, D. R. Justes, and A. W. Castleman, Jr., J. Phys. Chem. A **105**, 10237 (2001); A. Dinca, T. P. Davis, K. J. Fisher, D. R. Smith, and G. D. Willett, Int. J. Mass. Spectrom. **182/183**, 73 (1999); A. Fielicke and K. Rademann, Phys. Chem. Chem. Phys. **4**, 2621 (2002).

[5] H. Wu and L.-S. Wang, J. Chem. Phys. **108**, 5310 (1998); H. J. Zhai and L.-S. Wang, *ibid.* **117**, 7882 (2002).

[6] R. C. Bell, K. A. Zemski, K. P. Kerns, H. T. Deng, and A. W. Castlemann, Jr., J. Phys. Chem. A **102**, 1733 (1998).

[7] D. R. Justes, R. Mitric, N. A. Moore, V. Bonacic-Koutecký, and A. W. Castleman, Jr., J. Am. Chem. Soc. **125**, 6289 (2003).

[8] J. N. Harvey, M. Diefenbach, D. Schröder, and H. Schwarz, Int. J. Mass. Spectrom. **182/183**, 85 (1999).

[9] A. Pramann, K. Koyasu, A. Nakajima, and K. Kaya, J. Chem. Phys. **116**, 6521 (2002).

[10] K. R. Asmis, M. Brümmer, C. Kaposta, G. Santambrogio, G. von Helden, G. Meijer, K. Rademann, and L. Wöste, Phys. Chem. Chem. Phys. **4**, 1101 (2002).

[11] A. Fielicke, R. Mitric, G. Meijer, V. Bonacic-Koutecky, and G. von Helden, J. Am. Chem. Soc. **125**, 15716 (2003).

[12] M. Brümmer, C. Kaposta, G. Santambrogio, and K. R. Asmis, J. Chem. Phys. **119**, 12700 (2003).

[13] G. von Helden, A. Kirilyuk, D. van Heijnsbergen, B. Sartakov, M. A. Duncan, and G. Meijer, Chem. Phys. **262**, 31 (2000).

[14] O. Hübner and J. Sauer, Phys. Chem. Chem. Phys. **4**, 5234 (2002).

[15] M. Pykavy, C. van Wüllen, and J. Sauer, J. Chem. Phys. (to be published).

[16] A. D. Becke, J. Chem. Phys. **98**, 5648 (1993).

[17] S. F. Vyboishchikov and J. Sauer, J. Phys. Chem. A **104**, 10913 (2000).

[18] S. F. Vyboishchikov and J. Sauer, J. Phys. Chem. A **105**, 8588 (2001).

[19] G. K. Koyanagi, D. K. Bohme, I. Kretzschmar, D. Schröder, and H. Schwarz, J. Phys. Chem. A **105**, 4259 (2001).

[20] M. Calatayud, B. Silvi, J. Andrés, and A. Beltrán, Chem. Phys. Lett. **333**, 493 (2001).

[21] M. Calatayud, J. Andrés, and A. Beltrán, J. Phys. Chem. A **105**, 9760 (2001).

[22] J. Sauer and S. F. Vyboishchikov, poster presented at the Berichtskolloquium Sfb 546, Humboldt-Universität zu Berlin, February, 2002 (unpublished).

[23] D. Oepts, A. F. G. van der Meer, and P. W. van Amersfoort, Infrared Phys. Technol. **36**, 297 (1995).

[24] R. Ahlrichs, M. Bär, M. Häser, H. Horn, and C. Kölmel, Chem. Phys. Lett. **162**, 165 (1989); O. Treuler and R. Ahlrichs, J. Chem. Phys. **102**, 346 (1995); K. Eichkorn, O. Treutler, H. Öhm, M. Häser, and R. Ahlrichs, Chem. Phys. Lett. **242**, 652 (1995).

[25] A. D. Becke, Phys. Rev. A **38**, 3098 (1988).

[26] C. Lee, W. Yang, and R. G. Parr, Phys. Rev. B **37**, 785 (1988).

[27] P. J. Stephens, F. J. Devlin, C. F. Chabalowski, and M. J. Frisch, J. Phys. Chem. **98**, 11623 (1994).

[28] R. H. Hertwig and W. Koch, Chem. Phys. Lett. **268**, 345 (1997).

[29] A. Schäfer, C. Huber, and R. Ahlrichs, J. Chem. Phys. **100**, 5829 (1994).

[30] A. J. Wachters, J. Chem. Phys. **52**, 1033 (1970).

[31] P. Deglmann, F. Furche, and R. Ahlrichs, Chem. Phys. Lett. **362**, 511 (2002).

[32] A. P. Scott and L. Radom, J. Phys. Chem. **100**, 16502 (1996).

[33] M. D. Halls, J. Velkovski, and H. B. Schlegel, Theor. Chem. Acc. **105**, 413 (2001).

[34] S. A. Nizkorodov, J. P. Maier, and E. J. Bieske, J. Chem. Phys. **103**, 1297 (1995); D. Roth, O. Dopfer, and J. P. Maier, Phys. Chem. Chem. Phys. **3**, 2400 (2001).

[35] E. J. Bieske and O. Dopfer, Chem. Rev. (Washington, D.C.) **100**, 3963 (2000).

[36] J. M. Dyke, B. W. J. Gravenor, M. P. Hastings, and A. Morris, J. Phys. Chem. **89**, 4613 (1985).

[37] M. Pykavy and C. van Wüllen, J. Phys. Chem. A **107**, 5566 (2003).

[38] J. Harrington and J. C. Weisshaar, J. Phys. Chem. **97**, 2809 (1992).

[39] A. Fielicke, G. Meijer, and G. von Helden, J. Am. Chem. Soc. **125**, 3659 (2003).

[40] F. D. Hardcastle and I. E. Wachs, J. Phys. Chem. **95**, 5031 (1991).

[41] P. Clauws and J. Vennik, Phys. Status Solidi B **76**, 707 (1976).

[42] R. Enjalbert and J. Galy, Acta Crystallogr., Sect. C: Cryst. Struct. Commun. **42**, 1467 (1986).

[43] Calatayud, Andrés, and Beltrán (Ref. 21) incorrectly label the ground state of $V_2O_5^+$ $^2A''$. However, from the agreement of the bond distances and vibrational frequencies reported in Ref. 21 with our $^2A'$ results we gather that the state calculated was in fact the correct $^2A'$ ground state.